Li + HF: A Case Study to Develop Novel Computational Technologies for Reactive Scattering†

Antonio Laganà* and Stefano Crocchianti

Dipartimento di Chimica, Università di Perugia, Perugia, Italy

Received: September 27, 2000; In Final Form: November 29, 2000

The study of the Li + HF reaction has represented a laboratory for the development of theoretical and computational tools useful for the study of reaction dynamics of small molecules. The nature of these developments and their impact on future studies of chemical reactivity are discussed here.

Introduction

The study of the reactive properties of atom−diatom systems has accompanied not only the development of the understanding of reactive processes but also the evolution of several computational technologies. The Li + HF system can be considered as a suitable prototype of atom−diatom reactions because it is constituted of three different atoms and has a strongly bent transition state. The Li + HF system is, in fact, light enough to be computationally affordable and complex enough to show dynamical features common to larger systems whose theoretical studies are still out of reach when using rigorous quantum mechanical (QM) approaches. For this reason the Li + HF reaction has attracted much attention from both experimentalists and theorists. Up to date detailed crossed beam experiments[1,2] as well as classical (QCT)[3−8] and QM[9−16] theoretical studies have been reported in the literature.

The theoretical study of the Li + HF reaction and the use of exact quantum time independent methods based on hyperspherical coordinates are a focal point of our research. The visit paid by one of us (A.L.) to Aron Kuppermann in Caltech during the summer of 1982 was of fundamental importance for starting this research in our laboratory. It was, in fact, an opportunity to learn about the use of hyperspherical coordinates for three-dimensional exact quantum calculations and to hear about the just developing innovative design of parallel computing architectures.

Since then, the Li + HF reaction has become a case study for developing theoretical and computational technologies that are useful for the investigation of the reactivity of elementary chemical reactions. Such an investigation has allowed interesting developments in constructing potential energy surfaces (PES) and exploiting new ways of integrating quantum reactive scattering equations (see section 2). Here, we discuss the results of nonzero total angular momentum computations that are useful to establish possible links between the increase of the total angular momentum quantum number *J* and the variation of reactive properties (see section 3). Finally, related computational procedures are examined as test beds for the exploitation of parallel models and innovative problem-solving environments for reactive scattering applications (see section 4). Some conclusions are drawn in section 5.

† Part of the special issue "Aron Kuppermann Festschrift".

Methodological Advances

A great deal of advance in the study of atom−diatom reactions has been produced in providing functional formulations for potential energy surfaces. The first potential energy surface developed for the Li + HF system is the diatomic in molecule[17] surface, the quality of which was, however, insufficient to support dynamical calculations at the desired level of accuracy. For this reason, ab initio potential energy values were calculated[18] and a fit to a many body expansion (MBE) formulation of the interaction based on a generalized Rittner−Ridberg functional form was carried out.[19] Later on, a different MBE fitting procedure making use of a polynomial in bond order (BO) coordinates was adopted. The procedure converges to proper limiting values, and simple local corrections were used to correct occasional short-range spurious features.[8] Available ab initio potential energy values were integrated by points calculated using higher level approaches.[20] The PES obtained in this way was used for both quasiclassical[8] and quantum calculations.[15,21]

A novelty of this approach is the use of BO coordinates[22] or of their products with internuclear distances (RBO).[23,24] An advantage of BO space over the physical space is the collapse of infinite distances into the BO axis origin and the confinement of the interaction space into finite limits (zero internuclear distances correspond to a finite value of the related BO coordinate). Another advantage of variables defined in the BO space (more precisely their hyperspherical analogues) is the possibility of describing a reactive process (say A + BC → AB + C) using a rotating BO model (ROBO).[25] The ROBO model is conceptually simple to generalize to multiprocess reactions (LAGROBO)[26] and to polyatomic systems.[27,28] In these cases, the interaction of each elementary process is formulated as a rotating diatomic-like potential having parameters that vary with the rotation angle. BO coordinates show also features that are relevant to an alternative formulation of the scattering equations. They have been considered, in fact, both for formulating the basis set of the wave function expansion in a time independent approach to reactive scattering[29] and for grid representing the wave packet in the corresponding time dependent approach.[30]

Most of the dynamical calculations of the Li + HF reaction have up to now been carried out using QCT techniques. However, this system has also provided an ideal test bed for

10.1021/jp003506c CCC: $20.00 © 2001 American Chemical Society
Published on Web 02/20/2001

developing the quantum formalism, novel numerical approaches as well as innovative computational algorithms, parallel models, and computing environments. The first step forward to go beyond a QCT treatment of the Li + HF reaction has been the use of reduced dimensionality (RD) QM methods. These have allowed, for example, a rationalization of why the cross section increases when collision energy decreases at threshold and why isotopic substitutions for F and H have an opposite effect on the value of the reaction probability.[9,10]

A definite advance in the understanding of the reactive behavior of this system, however, can be provided only by the implementation of efficient exact 3D QM computational procedures. Yet, the implementation of these procedures is neither easy nor fast (first results were given in refs,[11,12,14] and work is still in progress[21,31]). Often memory and disk limitations represent a severe obstacle to the achievement of convergence. Sometimes, the limitation is given by the large amount of computing time associated with the calculations. Our work has also progressed along the 3D QM time dependent line[16,32] and along the appropriate transformation of the **S** matrix to evaluate stereodynamical properties.[33−35]

The work reported here focuses on the effect of increasing J on the dynamical outcome in order to provide useful hints to evaluate the efficacy of some popular approximations. The related formalism has been developed by expanding, as usual, the partial wave functions $\Psi^{JMpn}(\rho,\theta,\chi)$ (where J is the total angular momentum quantum number, M is its space fixed projection on the reference axis, p is the parity of the function, n is the numbering index of the partial waves, ρ is the hyperradius, θ and χ are the two internal hyperangles) expanded in terms of products of the Wigner rotation functions $\hat{D}^{Jp}_{\Lambda M}(\alpha,\beta,\gamma)$ times the corresponding surface functions $\Phi^{Jp}_{t\Lambda}$ (where Λ is the projection of the total angular momentum on the body fixed reference axis, t is the expansion index, α, β, and γ are the three Euler angles) calculated at fixed (ρ_ξ) value of ρ.[36] The key scattering information is carried by the expansion coefficients $\psi^{Jpn}_{t\Lambda}(\rho)$, which are functions of the hyperradius and whose asymptotic values can be obtained by integrating the coupled differential equations:

$$\left[\frac{\partial^2}{\partial\rho^2}+\frac{2\mu E}{\hbar^2}\right]\psi^{Jpn}_{t\Lambda}(\rho)=\frac{2\mu}{\hbar^2}\sum_{t'\Lambda''}\langle\Phi^{Jp}_{t\Lambda}\hat{D}^{Jp}_{\Lambda M}|H_I|\,\Phi^{Jp}_{t'\Lambda''}\hat{D}^{Jp}_{\Lambda'' M}\rangle\psi^{Jpn}_{t'\Lambda''}(\rho) \quad (1)$$

where E is the total energy and μ is the reduced mass of the system. As suggested by Launay,[37] the calculation of $\Phi^{Jp}_{t\Lambda}$ is performed once at a reference value $\bar{J}$ of the total angular momentum quantum number. In this case the surface functions are calculated by solving the equation

$$\left[T_h+\frac{15\hbar^2}{8\mu\rho_\xi^2}+\hbar^2G\bar{J}(\bar{J}+1)+\hbar^2C\Lambda^2+V(\rho_\xi,\theta,\chi)-\epsilon^{Jp}_{t\Lambda}(\rho_\xi)\right]\Phi^{Jp}_{t\Lambda}(\theta,\chi;\rho_\xi)=0 \quad (2)$$

and the internal Hamiltonian H_I of equation 1 is expressed as

$$H_I=T_h+T_r+T_c+\frac{15\hbar^2}{8\mu\rho^2}+V(\rho,\theta,\chi)+\hbar^2G[J(J+1)-\bar{J}(\bar{J}+1)-\Lambda^2]$$

where

$$T_\rho=\frac{\hbar^2}{2\mu\rho^5}\frac{\partial}{\partial\rho}\rho^5\frac{\partial}{\partial\rho}$$

$$T_h=\frac{\hbar^2}{2\mu\rho^2}\left(\frac{4}{\sin 2\theta}\frac{\partial}{\partial\theta}\sin 2\theta+\frac{1}{\sin^2\theta}\frac{\partial^2}{\partial\chi^2}\right)$$

$$T_r=A(\rho,\theta)J_x^2+B(\rho,\theta)J_y^2+C(\rho,\theta)J_z^2,$$

and

$$T_c=\frac{i\hbar\cos\theta}{\mu\rho^2\sin^2\theta}J_y\frac{\partial}{\partial\chi}$$

(subscripts "*h*", "*r*" and "*c*" stand for "hypersphere", "rotational," and "Coriolis", respectively). The constants *A*, *B*, *C* and *G* are defined as $A^{-1}(\rho,\theta)=\mu\rho^2(1+\sin\theta)$; $B^{-1}(\rho,\theta)=2\mu\rho^2\sin^2\theta$; $C^{-1}(\rho,\theta)=\mu\rho^2(1-\sin\theta)$; and $G=(A+B)/2$.

Obviously, the previously used computer codes had to be modified accordingly.[38] They are also being modified to incorporate the formalism of the tangent sphere coordinates, which smoothly transform from the Delves hyperspherical to the related Jacobi coordinates.[39] This makes it easier to impose the boundary conditions at large ρ values and calculate the detailed **S** matrix elements and related probabilities.

Reaction Properties

As already mentioned, some results of our 3D QM time independent investigation of the Li + HF reaction have been already reported in the literature.[11,12,21,31] Here we discuss the implications of extending the calculations to higher J values. The first set of results is shown in Figure 1. In the figure, state selected reactive probabilities (summed over all product quantum numbers) calculated at $J = 0$ (solid line), $J = 1$ (crosses connected by dotted lines), and $J = 2$ (circles connected by dashed lines) for the ground reactant vibrational state $v = 0$ and increasing values of the rotational state j (going from the bottom to the top panel) are plotted as a function of total energy E. It is worth pointing out here that, starting with $J = 2$, all terms of the internal Hamiltonian contribute to the propagation.

The solid line shows the detailed structure of the energy dependence of the $J = 0$ reactive probabilities calculated at a very fine energy grid (in steps of 0.0005 eV). The structure results from a combination of features associated with indirect collisions (linked to the bound states supported by the wells formed by the adiabats) and features associated with more direct collisions.[15] The association of the structure of the probability plots with quasibound states and indirect reaction mechanisms was confirmed by QCT[40] and QM[33,34] stereodynamics studies. The plot of Figure 1 shows also that the value of the total energy at threshold increases with the initial rotational quantum number j, implying that the energy supplied as reactants' rotation is not fully suitable to promote reaction.

For practical reasons, it was impossible to use the same energy grid for the higher J calculations. These were performed by varying E in steps of 0.030 eV. This coarser grid, however, though being unable to describe the fine structure of the energy dependence of the reactive probability is still sufficient to evaluate the different contributions of the various J terms to several reactive properties. As shown by the figure, the average contribution to reaction from single J probabilities at $j = 0$ is

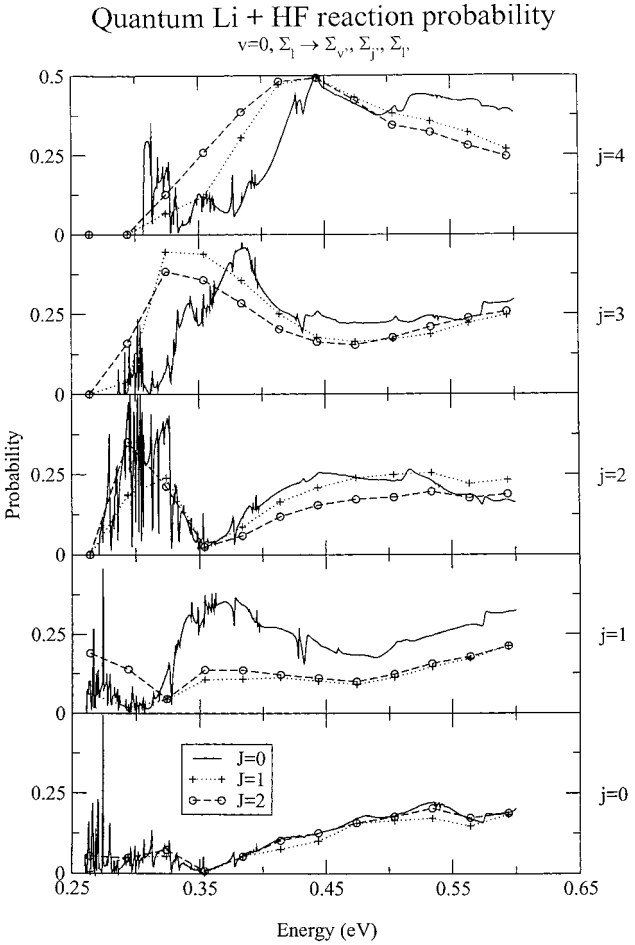

Figure 1. Reaction probabilities summed over all product states and reactant l states calculated at $v = 0$ and at j values ranging from 0 to 4 (from lower to upper panel) for $J = 0$ (solid line), $J = 1$ (dotted line with crosses) and $J = 2$ (dashed line with circles) plotted as a function of total energy E.

about the same, regardless of the value of the total angular momentum. Occasionally, mainly for energies lower than 0.35 eV, some $J = 0$ spikes exhibit large differences from the values calculated at $J = 1$ and $J = 2$. At larger energies, $J = 0$ results are slightly larger than those calculated at $J = 2$ (which, in turn, are slightly larger than those calculated at $J = 1$). These differences, however, may well be considered to fall within the error of the computation that was found to be of a few percent.

When reactants are rotationally excited, differences between contributions calculated at different J values are definitely larger and clearly beyond the error of the computation. The largest differences occur in the region adjacent the threshold more than at high energy. The largest difference occurs between $J = 0$ and higher J results, with $j = 1$ probabilities being responsible for most of it.

An objective of our study is to investigate when one can safely interpolate with energy the **S** matrix elements (this is necessary when applying a quantum number shift, as is the case of the J -shifting model[13,41]). In a J -shifting model, the unknown reactive state-to-state **S** matrix term $S^J_{vjl,v'j'l'}(E_{\mathrm{tr}})$ of the integral reactive cross section

$$\sigma_v(E_{\mathrm{tr}}) = \sum_j \frac{\pi(2j+1)\mathrm{e}^{-\epsilon_j/k_{\mathrm{B}}T}}{k^2_{vj}Q_{\mathrm{rot}}} \sum_J (2J+1) \sum_{v'j'} P^J_{vj,v'j'}(E_{\mathrm{tr}}) \quad (3)$$

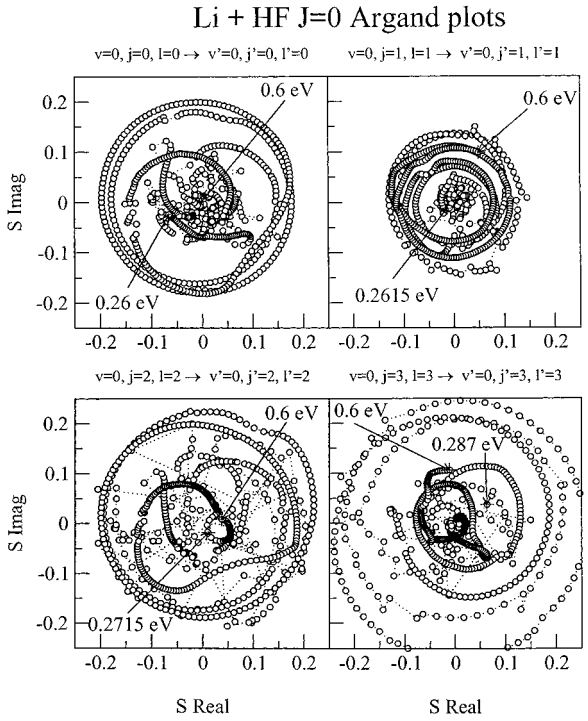

Figure 2. Argand diagrams for the J=0, v=v'=0 and j=j'=l=l'=0 (upper left panel), j=j'=l=l'=1 (upper right panel), j=j'=l=l'=2 (lower left panel), j=j'=l=l'=3 (lower right panel), reactive **S** matrix elements calculated at E =0.354 eV.

(E_{tr} is the translational energy and $P^J_{vj,v'j'}(E_{\mathrm{tr}})$ is the sum over l and l' of all the $|S^J_{vjl,v'j'l'}(E_{tr})|^2/[2(min(J,j)) + 1]$ terms where primed quantities are for products) can be expressed in terms of the element $S^{J*}_{vjl,v'j'l'}(E^{J,J*}_{tr})$ calculated at different reference J* and $E^{J,J*}$ values. To inspect the accuracy of the interpolation of the **S** matrix elements from the two nearest points, we have plotted the **S** matrix elements in the complex plane (Argand diagrams). Typical Argand diagrams related to the four lowest v=v'=0 j=j'=l=l' **S** matrix elements calculated at $J = 0$ are given in Figure 2. As apparent from the figure, in these cases the energy grid is fine enough to allow, in general, a straightforward interpolation of the radius of the polar representation that corresponds to the probability appearing in eq 3.

However, the J-shifting model works more properly when applied only to the highest terms of eq 3 (i.e., when the lowest terms are calculated directly from scattering equations). This is the case of our calculations for which exact quantum results are used for $J = 0$, $J = 1$, and $J = 2$. **S** matrix elements calculated at $J = 2$ are then used for the shifting. Fortunately, the smoothness of the Argand diagrams implies also a smoothness of the reaction probability plots, even when the energy grid is made coarser (as is the case of our non zero J calculations). This is confirmed by the fact that our calculations not only reproduce the high energy absolute value of the measured cross section of ref 1 but also predict the more detailed energy dependence of the recent measurements of Loesch,[42] including the spike at threshold.

Yet, before extending this approach to the calculation of the steric properties (such as the differential cross section) that require an interpolation with energy of both the real and the imaginary component of the **S** matrix elements, we investigated whether the energy grid used for our non zero J calculations is fine enough to allow an accurate interpolation. The grid size of 0.0005 eV used for $J = 0$ calculations confirms again to be fine enough. In fact, the solid and dashed line

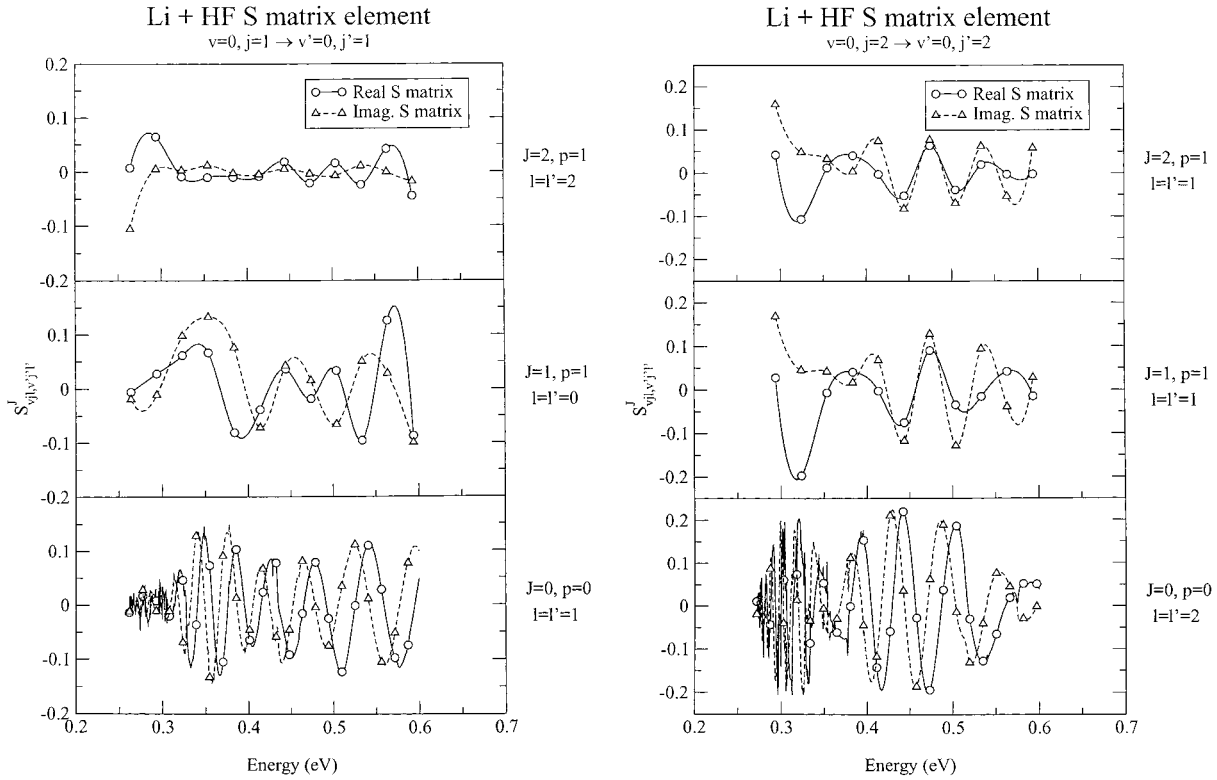

Figure 3. Imaginary (dashed line) and real (solid line) components of the **S** matrix elements calculated at $j=j'=l=l'=1$ (part *a*) and $j=j'=l=l'=2$ (part *b*) for $E = 0.354$ eV and $J = 0$ (bottom panels), $J = 1$ (central panels) and $J = 2$ (top panels). In the bottom panels plotted curves are generated from values calculated on an energy grid size of 0.0005 eV and open symbols indicate values obtained from a grid size of 0.015 eV. In the central and top panels, opens symbols indicate values calculated on a grid size of 0.03 eV whereas the curves are obtained from a spline fitting.

curves plotted in the bottom panel of Figure 3a,b where the imaginary and the real components of the $S^{J=0}_{v=0j=1l=1,v'=0j'=1l'=1}$ and $S^{J=0}_{v=0j=2l=2,v'=0j'=2l'=2}$ are plotted, show that there are enough points to give a detailed description of the energy dependence. The two curves show, in fact, a regularly oscillating behavior having an amplitude slowly varying with energy and a width slightly increasing with energy. This structure is still sufficiently well described, even when using a grid 10 times coarser (open circles and triangles in the same panels) though only at the highest energies. The figure shows, in fact, that the grid is completely inadequate to describe the structure of the curves in the low energy region.

The grid size used for our nonzero J calculations was even larger (0.03 eV). This explains why, as can be clearly seen from the central and top panels of Figure 3a,b, the solid and dashed line curves fitting the calculated values (open symbols) are unable to build a regular structure comparable with that of the $J = 0$ calculations. As a consequence, before extending the J shifting treatment to steric properties, additional non zero J calculations need to be performed.

To further investigate the reactive dynamics of the Li + HF reaction, we have analyzed also the way energy is disposed into product modes by plotting product energy distributions. In Figure 4, the product vibrational distributions (PVD) averaged over the detail of the rotational structure calculated at $v = 0$ and various j values ($j = 0$ (lower left panel), $j = 1$ (lower right panel), $j = 2$ (central left panel), $j = 3$ (central right panel), $j = 4$ (upper left panel), $j = 5$ (upper right panel)) for $J = 0$ and parity $p = 0$ (solid line with crosses), $J = 1$ and parity $p = 1$ (dotted line with empty triangles), $J = 2$ and parity $p = 1$ (dashed line with empty circles), $J = 5$ and parity $p = 1$ (dashed−dotted line with empty squares) are plotted, as usual, as a function of v'.

As is apparent from Figure 4, the $J = 0$ contribution to the PVD is not only, in general, the largest but also the one extending to the highest v' value. The $J = 0$ reactive probability is particularly large for $j = 1$ and $j = 3$. However, while for $j = 1$ the contributions from the other J values are small (the only appreciable contribution is from $J = 5$), for $j = 3$ contributions from $J = 1$, 2, and 5 are all comparable with the $J = 0$ one. A common feature of all distributions is, however that they are single peaked with a maximum at $v' = 0$.

Product rotational distributions (PRD) have also been determined for the two appreciably populated product vibrational states $v' = 0$ and $v' = 1$ (the probability of $v' = 1$ being, however, about 10 times smaller than that of $v' = 0$). The PRD of $v' = 0$ is shown in Figure 5. The $J = 0$ contribution to this PRD has the same structure, regardless of the initial rotational state (at least when the reaction probability is larger than the error of the computation). In particular, it has a maximum at $j' = 0$, $j' = 3$, and $j' = 5$, and it gives rise to a shoulder extending up to $j' = 14$ at larger product rotational states. The $J = 1$ component of the PRD shows a similar structure that, however, shifts the location of the peaks with j (e.g. for $j = 1$ the first maximum is located at $j' = 1$ while for $j = 3$ the first maximum is located at $j' = 0$). Even less regular is the behavior of the $J = 2$ component of the PRD. In fact, after little contribution at $j = 1$ ($j = 0$ and $j = 2$ contributions to the PRD are small for all values of J) and $j = 3$, it becomes comparable with contributions obtained from other J values. At $j = 3$ the contribution to the PRD has an absolute maximum at $j' = 2$, while at $j = 4$ and 5 it has an absolute maximum at $j' = 1$. A more regular structure is, again, shown by the $J = 5$ contribution to the PRD. This has, in fact, a maximum at $j' = 5$, regardless of the value of j.

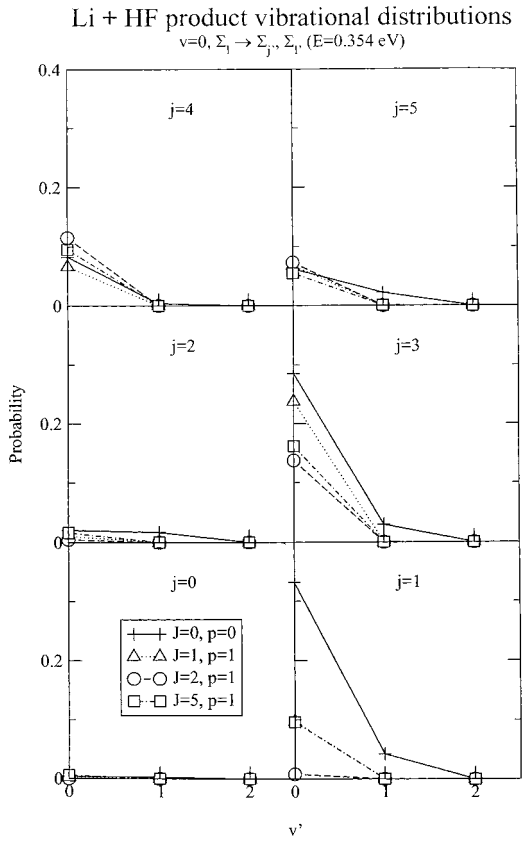

Figure 4. Product vibrational distributions (summed over product rotational states j') calculated at E = 0.354 eV, $v = 0$ and j values ranging from 0 to 5 (from the lower to the upper panels with even values on the left hand side and odd values on the right hand side) for $J = 0$ and parity $p = 0$ (solid line with crosses), $J = 1$ and parity $p = 1$ (dotted line with empty triangles), $J = 2$ and parity $p = 1$ (dashed line with empty circles), $J = 5$ and parity $p = 1$ (dashed−dotted line with empty squares).

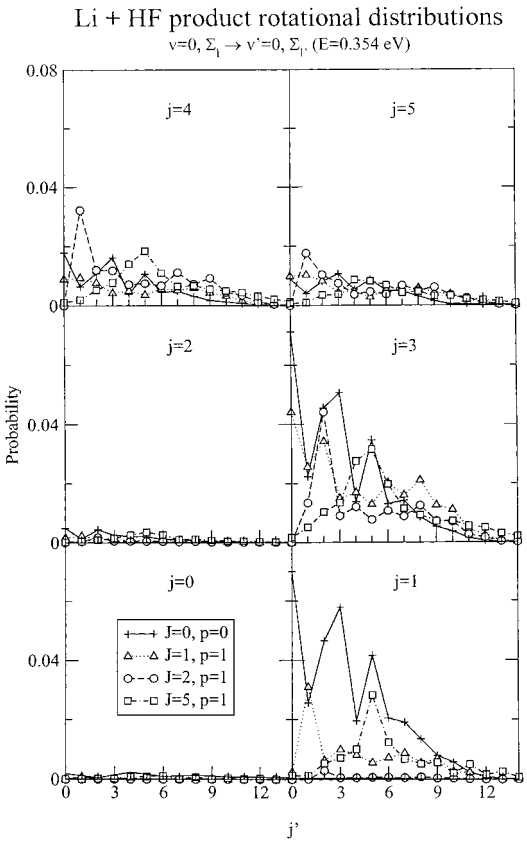

Figure 5. Product rotational distributions of the ground product vibrational state $v' = 0$ calculated at $E = 0.354$ eV, $v = 0$ and j values ranging from 0 to 5 (from the lower to the upper panels with even values on the left-hand side and odd values on the right-hand side) for $J = 0$ and parity $p = 0$ (solid line with crosses), $J = 1$ and parity $p = 1$ (dotted line with empty triangles), $J = 2$ and parity $p = 1$ (dashed line with empty circles), $J = 5$ and parity $p = 1$ (dashed−dotted line with empty squares).

The importance of the $J = 0$ component becomes even more apparent for the PRD of $v' = 1$ shown in Figure 6. The transition to this product vibrational state is quite small (it never exceeds 0.01). However, the $J = 0$ component is clearly the only appreciable contribution to the PRD and has systematically an absolute maximum at $j' = 3$, despite the fact that its value is smaller than the error of the computation.

Novel Computational Features

The implementation of the time-consuming part of the computational procedures on parallel machines is one of the innovative features that has accompanied the study of the Li + HF reaction. The exploitation of the parallelization has been already shown to speed up trajectory[43] and quantum reduced dimensionality[44] calculations.

The 3D QM time independent computational procedures are also speeded up significantly by parallelization. Our computational procedure is articulated into two main codes: ABM and LOGDER. ABM is devoted to solving the bound state problem of equation 2 that generates the fixed ρ_ξ eigenvalues $\epsilon_{t\Lambda}^{Jp}$ and the surface functions $\Phi_{t\Lambda}^{Jp}$, whereas LOGDER is devoted to the integration of the coupled differential equations 1.

ABM consists of two nested loops. The outer loop runs on the grid of the ρ_ξ values of the hyperradius chosen for the integration, whereas the inner loop runs on all possible values of Λ. The structure of the related algorithm is

```
Read input data
Calculate quantities of common use
LOOP on the hyperradius
  Calculate the actual value of ρξ
  LOOP on Λ
    Construct the basis set at the given ρξ
    Generate the surface functions at ρξ
    IF(i not 1) then
    Calculate overlaps between ρξ and ρξ−1 surface functions
      Store on disk the overlap matrix
    END IF
  END loop on Λ
  Calculate the coupling matrix
  Store on disk the coupling matrix
END loop on the hyperradius
```

As is apparent from the above scheme, the computation of the overlap matrix introduces an order dependency inhibiting parallelization.

Also, the serial version of LOGDER consists of two nested loops. As shown by the following scheme, the outer loop runs on E values, whereas the inner loop runs on the grid of ρ_ξ values.

```
Read input data
LOOP on energy E
  LOOP on the hyperradius
    Calculate the actual value of ρξ
    Step-propagate the solution
  END loop on the hyperradius
  Store the solution matrix
END loop on energy E
```

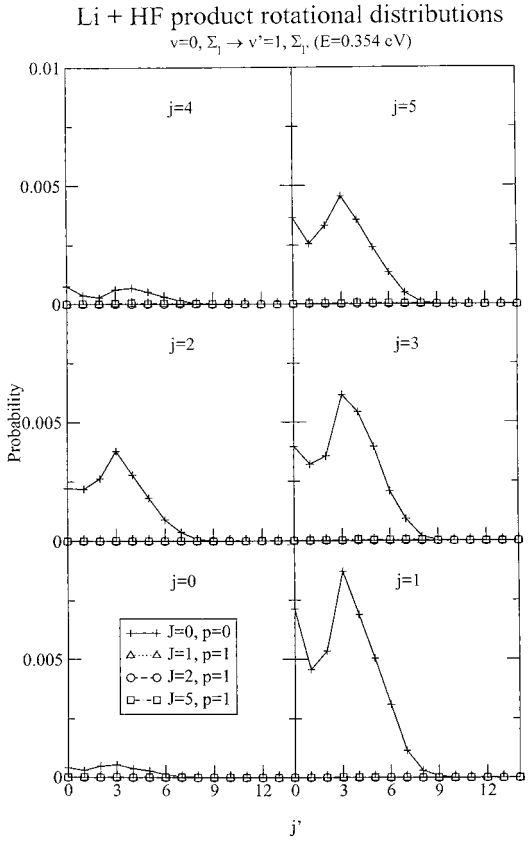

Figure 6. Product rotational distributions of the first excited product vibrational state $v' = 1$ calculated at $E = 0.354$ eV, $v = 0$ and j values ranging from 0 to 5 (from the lower to the upper panels with even values on the left-hand side and odd values on the right-hand side) for $J = 0$ and parity $p = 0$ (solid line with crosses), $J = 1$ and parity $p = 1$ (dotted line with empty triangles), $J = 2$ and parity $p = 1$ (dashed line with empty circles), $J = 5$ and parity $p = 1$ (dashed−dotted line with empty squares).

The step-propagation on the hyperradius makes the inner loop strictly recursive and, therefore, unsuitable for parallelization.

To parallelize ABM, the order dependency on ρ was eliminated by assigning blocks of ρ values to different nodes and by repeating for each block the calculation of the surface functions of the last ρ value of the previous block.[45] Better performances were obtained using a task farm[46] model with a dynamical balance of the work load (the calculation of the surface functions of any ρ value are assigned to the first available node[47]). According to this model, the structure of the master process is

```
Read input data
Send input data to all slaves
LOOP on the hyperradius
   Calculate the actual value of ρξ
   Call MPI_SEND(ρξ)
END loop on the hyperradius
```

The associated slave process is

```
Recv input data
10 Call MPI_RECV(ρξ)
Calculate the actual value of ρξ
LOOP on Λ
   Construct the basis set at ρξ
   Generate surface functions at ρξ
   Store on disk eigenvalues and eigenvectors
   Call MPI_BARRIER
   IF(i not 1) then
      Construct the basis set at ρξ−1
      Read eigenvectors at ρξ−1
      Compute overlap integrals
      Store on disk the overlap matrix
   END IF
END loop on Λ
Calculate the coupling matrix
Store on disk the coupling matrix
GOTO 10
```

LOGDER was also parallelized using a task farm at the level of the loop on E. Accordingly, the scheme of the master process is

```
Read input data
Send input data to all slaves
LOOP on energy E
   Call MPI_SEND(E)
END loop on energy E
```

The master process reads and broadcasts the input data to the worker processes. The work is assigned to the workers by sending the current energy value. The scheme of the slave process is

```
Recv input data
10 Call MPI_RECV(E)
LOOP on the hyperradius
   Calculate the actual value of ρξ
   Step-propagate the solution
END loop on the hyperradius
Store the solution matrix
GOTO 10
```

However, because the request of computing power for tackling problems of increasingly complexity grows faster than the computing power available on single-machine platforms (moreover, the tendency to build increasingly powerful top-end individual platforms is not as marked as in the past), a suitable solution is to cluster available computers (ranging from desk computers to extremely powerful parallel machines) to work cooperatively. These hardware and software solutions, often called metacomputing or cluster computing, are usually only one aspect of the effort needed to build an environment suitable for managing realistic simulations of complex chemical systems such as those of interest, as an example, for environmental modeling or spacecraft engineering. The complexity of the applications, in fact, requires also a gathering of several complementary expertises even to realize a single project and the construction of a software environment oriented toward the solution of the problem of interest.

Along this direction, the European Union has recently implemented an initiative (METACHEM) promoting the constitution of Metalaboratories[48] (clusters of research laboratories aimed at designing and implementing chemical software and connected via a metacomputer). This initiative takes advantage of the existing collaborative framework of COST (a European initiative for collaboration in science and technology) and exploits the Web as an infrastructure for designing and running coarse-grained distributed complex applications.[49,50]

In this context, the Web acts as a support for building smart, user-friendly problem-solving environments (PSE). PSEs enable the scientists to carry out their investigations without caring about the complexity of the computing platform. The PSE, in fact, uses a problem-oriented language that allows the user to run applications with no need to know the underlying computer hardware or software.[51]

A PSE devoted to the simulation of molecular beam experiments (SIMBEX), whose outlines have been given else-

where,[52,53] is going to be implemented as one of the projects of METACHEM. SIMBEX is articulated into three blocks devoted to (1) the construction of the potential energy surface, (2) the performing of dynamical calculations, and (3) the averaging and visualization of the outcomes on virtual monitors.

More in detail, if, as is the case of the Li + HF reaction, a suitable potential energy surface is not available, a fit to the ab initio potential energy values has to be performed. When ab initio potential energy values are insufficient or unavailable, a package carrying out either ab initio or semiempirical calculations needs to be activated in the first block (eventually after a proper adjustment of the values to reproduce known structural properties of the system and its fragments). SIMBEX, however, can also retrieve PES routines from the Web. The inclusion of multisurface treatments in which each surface is fitted to one functional form or to functional forms directly providing multiple solutions, is also being planned.

The second block of SIMBEX provides the integration of scattering equations. Dynamics calculations were performed (on a single or on a multiple surface) using either QCT or QM techniques (though the procedure for handling quantum calculations is still to a great extent handled manually by the user, especially in the initial phase of parameters tuning). The calculations provide a set of scattering **S** or probability **P** matrix elements with which to evaluate the properties of interest. From them, virtual monitors are built comparing calculated and measured quantities. To this end an averaging over the energy spread of the crossing beams, the integration over the collision volume, and the transformation from the CM to the laboratory frame are needed to reconstruct, in terms of solid angle and distance from the crossing point, the intensity of the product beam measured by a beam experiment.

The process can also be driven in the opposite direction to obtain from the measured intensity of the beam and the related velocity distribution the calculated energy and angular distributions of the products.

The related PSE[54] is structured so as to have a Web browser on the client side, a cluster of distributed computing resources as a back-end and a collection of Web servers as middleware.

Conclusions

The theoretical investigation of the Li + HF prototype reaction is continuously funneling innovation into methodological and computational approaches to chemical reactivity. On the methodological side, innovation discussed in this paper is concerned with the formulation of both the potential energy surface and the scattering equations. As for the formulation of the PES, the discussion has focused on the advantages associated with the use of BO coordinates for fitting available ab initio and experimental data, especially in view of their extension to polyatomic systems. As for the scattering equations, the discussion has focused on the recent evolutions of hyperspherical coordinates that have been used for the calculations reported here. Mention is also made to an alternative approach based non-orthogonal coordinates of the BO type.

Thanks to these methodological and computational advances, it has been possible to analyze the effect of increasing the value of the total angular momentum quantum number on the efficiency of reactive mechanisms and on the disposal of energy to products. Particular attention has been paid to the applicability of techniques requiring an interpolation in energy of the **S** matrix elements with respect to the grid size used.

The other contribution of the investigation of the Li + HF reaction is on the computer science side. The study of this reaction, in fact, has offered an opportunity for investigating the modern paradigms of computational chemistry. In particular, in this paper, parallel computing and problem-solving environments have been discussed. As for parallel computing, it has been shown that only an in-depth analysis of the computational code based on its physical and chemical foundations allows an efficient exploitation of the parallelism and a proper adoption of parallel models. At the same time, the crossed molecular beam study of the Li + HF reaction has also provided a suitable case study to design a problem-solving environment aimed at managing complex chemical applications on distributed computing platforms by gathering together complementary expertises and heterogeneous machines.

Acknowledgment. We acknowledge support to this work from EU through COST in chemistry (action D9 project 0003/98) and TMR (contract ERB FMGE CT95 0062 assigned to CESCA-CEPBA and contract ERB FMGE CT95 0051 assigned to EPCC) and from Italian MURST, CNR and ASI.

References and Notes

(1) Becker, C. H.; Casavecchia, P.; Tiedemann, P. W.; Valentini, J. J.; Lee, Y. T. *J. Chem. Phys.* **1980**, *73*, 2833.
(2) Loesch, H. J.; Stienkemeier, F. *J. Chem. Phys.* **1993**, *98*, 9570.
(3) Alvariño, J. M.; Casavecchia, P.; Gervasi, O.; Laganà, A. *J. Chem. Phys.* **1982**, *77*, 6341.
(4) Noorbatcha, I.; Sathyamurthy, N. *J. Am. Chem. Soc.* **1982**, *104*, 1766.
(5) Noorbatcha, I.; Sathyamurthy, N. *J. Chem. Phys.* **1983**, *77*, 67.
(6) Noorbatcha, I.; Sathyamurthy, N. *Chem. Phys. Lett.* **1982**, *93*, 432.
(7) Laganà, A.; Hernández, M. L.; Alvariño, J. M. *Chem. Phys. Lett.* **1984**, *106*, 41.
(8) Alvariño, J. M.; Hernández, M. L.; Garcia, E.; Laganà, A. *J. Chem. Phys.* **1986**, *84*, 3059.
(9) Laganà, A.; Aguilar, A.; Gimenez, X.; Lucas, J. M. *Chem. Phys. Lett.* **1992**, *189*, 138.
(10) Laganà, A.; Ochoa de Aspuru, G.; Aguilar, A.; Gimenez, X.; Lucas, J. M. *J. Phys. Chem.* **1995**, *99*, 11696.
(11) Parker, G. A.; Pack, R. T.; Laganà, A.; Archer, B. J.; Kress, J. D.; Bacic, Z. In *Supercomputer Algorithms for Reactivity, Dynamics and Kinetics of Small Molecules*; Laganà, A, Ed.; Kluwer: Dordrecht, 1989; p 105.
(12) Parker, G. A.; Pack, R. T.; Laganà, A. *Chem. Phys. Lett.* **1993**, *202*, 75.
(13) Laganà, A.; Parker, G. A.; Pack, R. T. *J. Chem. Phys.* **1993**, *99*, 2269.
(14) Baer, M.; Last, I.; Loesch, H. J. *J. Chem. Phys.* **1994**, *101*(11), 9648.
(15) Parker, G. A.; Laganà, A.; Crocchianti, S.; Pack, R. T. *J. Chem. Phys.* **1995**, *102*, 1238.
(16) Aguado, A.; Paniagua, M.; Lara, M.; Roncero, O. *J. Chem. Phys.* **1997**, *107*(23), 10085.
(17) Zeiri, Y.; Shapiro, M. *Chem. Phys.* **1978**, *31*, 217. Shapiro, M.; Zeiri, Y. *J. Chem. Phys.* **1979**, *70*, 5264.
(18) Chen, M. M. L.; Schaefer, H. F. *J. Chem. Phys.* **1980**, *72*, 4376.
(19) Carter, S.; Murrell, J. N. *Mol. Phys.* **1980**, *41*, 567.
(20) Palmieri, P.; Laganà, A. *J. Chem. Phys.* **1989**, *91*, 7303.
(21) Laganà, A.; Bolloni, A.; Crocchianti, S.; Parker, G. A. *Chem. Phys. Lett.* **2000**, *324*, 466.
(22) Garcia, E.; Laganà, A. *Mol. Phys.* **1985**, *56*, 629.
(23) Dini, M. *Proprietà delle superfici di energia potenziale e reattivita' chimica dei sistemi M + HX (M = IA, IIA e X = VIIA)*, Tesi di Laurea, Università di Perugia 1986. Laganà, A.; Dini, M.; Garcia, E.; Alvariño, J. M.; Paniagua, M. *J. Phys. Chem.* **1991**, *95*, 8379.
(24) Aguado, A.; Sieiro, C.; Paniagua, M. *J. Mol. Struct. (THEOCHEM)* **1992**, *260*, 179. Aguado, A.; Sieiro, C.; Paniagua, M. *J. Chem. Phys.* **1992**, *96*, 1625. Aguado, A.; Paniagua, M. *J. Chem. Phys.* **1992**, *96*, 1265. Aguado, A.; Suárez, C.; Paniagua, M. *J. Chem. Phys.* **1983**, *98*, 308.
(25) Laganà, A. *J. Chem. Phys.* **1991**, *95*, 2216.
(26) Laganà, A.; Ochoa de Aspuru, G.; Garcia, E. *J. Chem. Phys.* **1998**, *108*, 3886.
(27) Ochoa de Aspuru, G.; Clary, D. C. *J. Phys. Chem. A* **1998**, *102*, 9631.
(28) Gervasi, O., unpublished work.
(29) Laganà, A.; Spatola, P.; Ochoa de Aspuru, G.; Ferraro, G.; Gervasi, O. *Chem. Phys. Lett.* **1997**, *267*, 403.

(30) Ferraro, G.; Faginas Lago, N.; Laganà, A. *Reaction Dynamics in Bond Order Coordinates*, in preparation.

(31) Laganà, A.; Bolloni, A.; Crocchianti, S. *Phys. Chem. Chem. Phys.* **2000**, *2*, 535.

(32) Gögtas, F., Balint-Kurti, G. G.; Offer, A. R. *J. Chem. Phys.* **1996**, *104(20)*, 7927.

(33) Alvariño, J. M.; Aquilanti, V.; Cavalli, S.; Crocchianti, S.; Laganà, A.; Martinez, T. *J. Chem. Phys.* **1997**, *107*, 3339.

(34) Alvariño, J. M.; Aquilanti, V.; Cavalli, S.; Crocchianti, S.; Laganà, A.; Martinez, T. *J. Phys. Chem.* **1998**, *102*, 9638.

(35) de Miranda, M. P.; Crocchianti, S.; Laganà, A. *J. Chem. Phys.* **1999**, *103*, 10776.

(36) Pack, R. T.; Parker, G. A. *J. Chem. Phys.* **1987**, *87*, 3888.

(37) Launay, J. M.; LeDourneuf, M. *Chem. Phys. Lett.* **1989**, *163*, 178.

(38) Parker, G. A.; Crocchianti, S., unpublished work.

(39) Parker, G. A.; Crocchianti, S.; Keil, M. *Quantum Reactive Scattering for Three Particle Systems using Hyperspherical Coordinates*; Laganà, A.; Riganelli A., Eds., *Lecture Notes in Chemistry* **2000**, *75*, 88. Parker, G. A.; Keil, M.; Morrison, M. A.; Crocchianti, S. *J. Chem. Phys.* **2000**, *113*, 957.

(40) Alvariño, J. M.; Basterrechea, F. J.; Laganà, A. *Mol. Phys.* **1986**, *59*, 559.

(41) Bowman, J. M. *J. Chem. Phys.* **1991**, *95*, 4960.

(42) Höbel, O.; Menéndez, M.; Loesch, H. J. *Molec 2000*, Jerusalem 2000.

(43) Laganà, A.; Gervasi, O.; Baraglia, R.; Laforenza, D.; Perego, R. *Theor. Chim. Acta* **1992**, *84*, 413.

(44) Baraglia, R.; Laforenza, D.; Laganà, A. *Lecture Notes in Computer Science* **1995**, *919*, 554. Laganà, A.; Crocchianti, S.; Bolloni, A.; Piermarini, V.; Baraglia, R.; Ferrini, R.; Laforenza, D. *Comput. Phys. Comm.* **2000**, *128*, 295.

(45) Laganà, A.; Crocchianti, S.; Ochoa de Aspuru, G.; Gargano, G.; Parker, G. A. *Lecture Notes in Computer Science* **1995**, *1041*, 361.

(46) Pelagatti, S. *Structured development of parallel programs*, Taylor & Francis Ltd.: London, 1998.

(47) Bolloni, A.; Riganelli, A.; Crocchianti, S.; Laganà, A. *Lecture Notes in Computer Science* **1998**, *1497*, 331.

(48) Laganà, A. *METACHEM: Metalaboratories for cooperative innovative computational chemical applications*; METACHEM workshop, Brussels, Belgium, November 1999 (see also D23: Technical annex).

(49) Gentzsch, W. Ed., *Future Generation Computer Systems*, **1999**, *15*.

(50) Baker, M.; Buyya, R.; Laforenza, D. *The Grid: International Efforts in Global Computing*, SSGRR2000, L'Aquila, Italy, July 2000.

(51) Gallopoulos, S.; Houstis, E.; Rice, J. *Computer as Thinker/Doer: Problem-Solving Environments for Computational Science*, IEEE Computational Science and Engineering, Summer 1994.

(52) Gervasi, O.; Cicoria, D.; Laganà, A.; Baraglia, R. *Pixel* **1994**, *10*, 19.

(53) Laganà, A.; Gervasi, O. *A Structured Computational Approach to Chemical Reactivity for Problem-Solving Environments*, in preparation.

(54) Baraglia, R.; Laforenza, D.; Laganà, A. *A Web based Metacomputing Problem-Solving Environment for Complex Applications*, Workshop on Grid Computing, Bangalore, December 2000.